IRIS AperTO

UNIVERSITÀ DEGLI STUDI DI TORINO

AperTO - Archivio Istituzionale Open Access dell'Università di Torino

[M]-CAL-2: MeAPSO-34-like molecular sieves using a lamellar aluminophosphate as precursor

This is the author's manuscript

Original Citation:

Availability:

This version is available http://hdl.handle.net/2318/146397 since 2016-10-03T11:15:14Z

Published version:

DOI:10.1016/j.micromeso.2013.12.020

Terms of use:

Open Access

Anyone can freely access the full text of works made available as "Open Access". Works made available under a Creative Commons license can be used according to the terms and conditions of said license. Use of all other works requires consent of the right holder (author or publisher) if not exempted from copyright protection by the applicable law.

(Article begins on next page)

04 May 2023

UNIVERSITÀ DEGLI STUDI DI TORINO

This Accepted Author Manuscript (AAM) is copyrighted and published by Elsevier. It is posted here by agreement between Elsevier and the University of Turin. Changes resulting from the publishing process - such as editing, corrections, structural formatting, and other quality control mechanisms - may not be reflected in this version of the text. The definitive version of the text was subsequently published in

Microporous and Mesoporous Materials, Vol. 187, 6 January 2014
DOI: 10.1016/j.micromeso.2013.12.020

You may download, copy and otherwise use the AAM for non-commercial purposes provided that your license is limited by the following restrictions:

(1) You may use this AAM for non-commercial purposes only under the terms of the CC-BY-NC-ND license.

(2) The integrity of the work and identification of the author, copyright owner, and publisher must be preserved in any copy.

(3) You must attribute this AAM in the following format: Creative Commons BY-NC-ND license (http://creativecommons.org/licenses/by-nc-nd/4.0/deed.en),

http://dx.doi.org/10.1016/j.micromeso.2013.12.020

[M]-CAL-2: MeAPSO-34-like molecular sieves using a lamellar aluminophosphate as precursor

Mathias Strauss[1], Gesley Alex Veloso Martins[2], Gloria Berlier[2], Salvatore Coluccia[2], Leonardo Marchese[3], Heloise O. Pastore[1,*]

[1]Micro and Mesoporous Molecular Sieves Group, Institute of Chemistry, University of Campinas, Rua Monteiro Lobato, 270, 13083-861, Campinas, SP, Brazil.

[2] Università di Torino, Dipartimento di Chimica and NIS Centre of Excellence, Via P. Giuria 7, 10125 Torino, Italy

[3]Dipartimento di Scienze e Tecnologie Avanzate and Centro Interdisciplinare Nano-SISTEMI, Universitá del Piemonte Orientale, Via Bellini 25G, 15100 Alessandria, Italy.

*gpmmm@iqm.unicamp.br

ABSTRACT

[M]-CAL-2 (M = Mn, Co and Fe) are metallosilicoaluminophosphates ([M]-APSO) with chabazite-related structure, which are part of the CAL molecular sieves family. They were prepared with a recently developed synthesis based on the use of layered AlPO precursor. The used procedure allowed to obtain high loadings of metal ions and to control the morphology of the crystals. The materials were characterized by structural techniques such as X-ray diffraction, scanning electron microscopy (SEM), energy dispersive spectroscopy (EDS), thermogravimetry (TGA), and spectroscopic techniques such as UV-Vis and Fourier transformed Infrared (FTIR) with particular attention to the study of their redox functionalities. The results show that [M]-CAL-2 crystals presented rhombohedra morphology and the particles sizes are dependent of the metal concentration in the precursor gel, in addition these particles have a lamellar memory originated from the layered AlPO precursor. The FTIR, UV-Vis and elemental results supported the presence of transition metal ions on the framework of the synthesized materials and allowed to envisage the dependency of the metal and silicon concentrations on a Lowenstein-like ruled substitution mechanism. Finally, the reversible redox behavior of the materials was studied by in situ UV-vis-NIR spectroscopy. This aspect together with the already shown acidity of CAL samples

allowed confirming the acid and redox bifunctionality of the obtained molecular sieves, which can thus be proposed for catalytic applications

INTRODUCTION

The microporous materials have been widely studied due to their properties as catalysts, molecular sieves and ions exchangers especially related to their well defined pores, channels and cavities as well as to their chemical composition. The most known example of this kind of materials are zeolites and zeotypes, aluminophosphates (AlPOs) and silicoaluminophosphates (SAPOs).

Normally these materials are prepared by a sol-gel synthesis route where the silicon, aluminium and/or phosphorous sources (depending on the final material chemical composition) are dissolved or suspended in a solvent (water is the most used) and mixed until the obtained reaction media is perfectly homogeneous. At the end a structure directing agent (SDA) may be added that will be responsible for the final structure of the microporous material. Another explored synthesis protocol to prepare these materials is the use of a natural or synthetic clay as single source of aluminum and silicon. The use of synthetic clays has not been encouraged due to several contamination problems, especially with iron [1], related to the use of their natural analogues.

It is well known that several SAPOs and AlPOs may be synthesized from a lamellar intermediate during the hydrothermal treatment of their synthesis gel [2-6]. This behavior opened a great opportunity on the use of lamellar single-source materials on the synthesis of various SAPOs and AlPOs. However this road remained unexplored until the report of a layered aluminophosphate (AlPO-ntu) isostructural to the siliceous kanemite [7]. This lamellar aluminophosphate, herein designated as AlPO-kan, was then used as Al and P single-source in the synthesis of diverse SAPOs denominated as the CAL (acronym of CAmpinas-ALessandria) family molecular sieves [8]. After that, several SAPOs with different structures where obtained by varying the synthesis method always starting from AlPO-kan as precursor. Chabazite (CHA) structures, analogous to SAPO-34, where obtained and named as CAL-1[9,10] and CAL-2 [11]; another CHA structure, analogous to SAPO-44, was prepared and named CAL-4 [12,13]. A triclinic form of chabasite AlPO (CAL-5 [14]) and a levyne (LEV) structure material (CAL-3 [15]) were also obtained. Another study showed the influence of

tetraalkylammonium salts as SDAs on the final structure and crystals morphology of the CAL family related materials [16].

The CAL family materials prepared so far presented only acid properties. Accurate studies of the acidic behavior of these materials were previously described by Pastore et al. [8], and therefore their application, for example, in catalysis is restricted to the branch of acid catalysed reactions. The insertion of transition metals in T-positions in the framework could enlarge their application possibilities to redox catalytic reactions such as NO_x decomposition [17] or H_2 and methane combustion. The incorporation of transition metal atoms in the structure of SAPOs was first reported in 1986 [18,19] originating the MeAPSO materials, which are moreover characterized by a larger versatility in chemical structures with respect to zeolites. In order to open the possibilities of using the family CAL materials in redox-type catalytic reactions this work presents the synthesis and structural characterization of CHA-like MeAPSO-34 analogous molecular sieves with framework transition metal ions (Mn, Co and Fe) using the same synthetic approach used for the other CAL materials.

EXPERIMENTAL

AlPO-kanemite ($AlPO_3OH(CH_3(CH_2)_3NH_2)$) preparation [7]

The lamellar aluminophosphate used as Al and P single source in the synthesis of CAL solids was prepared as described by Cheng et al. [7] using butylamine, and reduced homogenization time of each step during the synthetic process as described before [16]. The material thus obtained is referred to as butNH_2-AlPO-kan.

[M]-CAL-2 synthesis

The [M]-CAL-2 was prepared using a modified procedure as the one described in Patent Application for the CAL-2 molecular sieve synthesis [11]. Silica Aerosil 200 was used as silicon source, with SiO_2/Al_2O_3 molar ratio of 1.0. The transition metal salts ($CoCl_2$, $MnCl_2$ or $Fe(NO_3)_3$) were added during the synthesis to the gel with M/Al_2O_3 molar ratio of 0.11, 0.22 or 0.33. The final gel was hydrothermally treated for 48 h. A typical synthesis of these materials was carried out as described below. ButNH_2-AlPO-kan (4.00 g), prepared as described above, was suspended in 16.9 mL of distilled water and stirred for 3 h in a propylene becker. After that, 0.56 g of silica (Aerosil 200, Degussa) were added and the gel was stirred for 1 h. Than the appropriate amount of the transition metal salt was added and the gel was stirred for one more hour. The reaction gel was

transferred to a Teflon lined, stainless steel autoclave, and maintained at 190 °C for 48 h. The final solid was then filtered and washed with copious amounts of distillated water. The samples in this work are named as [M]-CAL-2 (M = Co, Mn or Fe); these codes are accompanied by the M/Al_2O_3 molar ratio (0.11, 0.22 or 0.33).

Characterization methods

X-ray diffractometry (XRD)

Materials were characterized by X-ray diffraction using a Shimadzu equipment model XRD7000 with CuKα radiation (λ = 1.5418 Å), from 1.4° to 50° (2θ) at a rate of 2° 2θ min^{-1}, with 0.5°, 0.5° and 0.3 mm for output, divergence and reception slits, respectively, at room temperature.

Fourier transformed infrared spectroscopy (FTIR)

Infrared spectra were obtained using a Nicolet 6700 spectrophotometer at a resolution of 4 cm^{-1} at room temperature. The samples were prepared for analysis using the homogenous KBr mixture method with a 0.5 wt% dilution.

Scanning electron microscopy (SEM) and framework elemental analysis

SEM images were obtained using a JEOL 6360-LV microscope with thermoionic cannons operating at 20 kV. Samples were examined after gold sputtering at a Bal-Tec MED-020. Images were acquired using secondary electrons and were analyzed by Energy dispersive spectroscopy (EDS) using a carbon sample holder covered with a carbon layer by a Voltec evaporator, in a NORAN Instruments Spectrometer coupled with the JEOL 6360-LV microscope.

Thermogravimetry (TGA)

The samples were analyzed in TA Instruments 2950 Model equipment under air flow (100 mL min^{-1}) from room temperature to 1273 K, at a heating rate of 10 K min^{-1}.

Diffuse Reflectance (DR) UV-Vis measurements

DR UV-Vis measurements were performed on previously calcined samples. Calcination was carried out in a tubular oven by charging about 1 gram of as-synthesized sample in an alumina sample holder. A flow of 100 mL min^{-1} of dry N_2 was employed while heating the sample until 723 K with a rate of 1 K min^{-1}. The sample was kept at this

temperature for 4 h under N_2, after that N_2 gas was gradually changed with O_2 and the temperature was increased until 923 K. The sample was left at this temperature for 5h.
For DR UV-Vis measurements, approximately 400 mg of material were charged in a tubular quartz cell with a quartz window, which was connected to a vacuum line to perform *in situ* oxidation and reduction treatments on previously outgassed samples. The oxidation was performed at 823 K (5 cycles of 20 Torr of O_2) and the reduction at 673 K (5 or more cycles of 20 Torr of H_2). The measurements were carried out in a Perkin-Elmer UV-Vis-NIR Spectrometer Lambda19 equipped with a $BaSO_4$ covered integrating sphere in the wavenumber range 4.000 – 50.000 cm^{-1}. $BaSO_4$ was used as reference.

RESULTS AND DISCUSSIONS

The comparison of the X-ray diffraction patterns of the materials obtained in this work with the CHA standard (Methylbutylamine SAPO-47, $|(C_5H_{12}NH_2)_{1.4}(H_2O)_{2.5}|[Al_{6.0}Si_{1.4}P_{4.6}O_{24}]$) from the International Zeolite Association (IZA)[20] (Figure 1) indicated that the obtained structure is the chabasite one, independently of the transition metal source ($CoCl_2$, $MnCl_2$ or $Fe(NO_3)_3$) and its molar ratio (M/Al_2O_3, M= Co, Mn or Fe) used during the preparation of the synthesis gel. The same kind of structure is obtained when no transition metal salt is used (CAL-2 XRD pattern in Figure 1); indicating that the metal ions (Co^{2+}, Mn^{2+} and Fe^{3+}) and their counter-ions (Cl^- and NO_3^-) do not have any influence as structure directing agents during the materials synthesis. No extra phases of crystalline nature are present. Well defined and narrow peaks indicate that the solids have good crystallinity, as discussed above.

The relative cristallinity (%C) of each materials group ([Co], [Mn] or [Fe]-CAL-2) is calculated from the sum of the integrated values of the four most intense peaks above 15° (2θ) (20.7, 24.8, 30.6 and 30.7°) for every diffractogram. The maximum crystallinity, 100% is assigned to the highest integration value, with the other percentages based on this value. The results are presented in Table 1.

The crystallinity behavior in each materials group shows that the highest concentrations of the transition metal used in the synthesis produced the least crystalline products, suggesting that the transition metal atoms are located at the crystalline

network and in different amounts related to their initial concentration in the synthesis gel.

Distortions in the crystalline network are probably created when these transition metal atoms are inserted in the structure of the silicoaluminophosphates because the M-O (M = Co, Mn or Fe) bond lengths (1.9-2.0Å) [21-23] are longer than the typical T-O (T = Si, Al or P) bond lengths of silicoaluminophosphates (1.5-1.7Å) [24,25]. The difference in the bond lengths affects also the bond angles from the MO_4 and TO_4 tetrahedra present as basic construction units at these materials creating distortions along the crystalline network and so lowering the materials' crystallinities. The tetrahedral geometry from the transition metal centers of these materials will be discussed more carefully using the UV-vis spectroscopy results.

The bands observed by infrared spectroscopy (IR) between 1400 and 400 cm^{-1} are commonly used to analyze the structural vibrations of the inorganic network of molecular sieves. In the case of MeAPSO-34 and the materials studied in this work, it is possible to observe bands attributed to symmetric and antisymmetric stretching of the TO_4 (T = Si, Al, P or M), as well as vibrations related to double 6-membered rings and 8-membered access windows typical to chabasite like materials [26].

The position of the bands observed in all the IR spectra of the synthesized materials coincide (Figure 2), indicating that the basic construction units and the short distance organization of the structure are identical for all the materials regardless of the type or concentration of the transition metal used during the synthesis. The attributions of the observed bands are presented in Table 2 and they correlate perfectly with the bands of CAL-2.

For all the materials the peaks at 2961, 2930 and 2874 cm^{-1}, shown in Figure 3a, are assigned to C–H stretchings and the absorptions at 1465 and 1544 cm^{-1} to CH bending from the n-butylammonium cation present at the chabazite cavities as structural directing agent (SDA). The presence of the signals at about 1600 and 1500 cm^{-1} is related to the presence of the alkylammonium ion [27] these signals are attributed to the N–H bending at NH_3^+ and their presence indicates that the amine is protonated and is present as counter-cation of the structural negative charges in the final materials [7].

All the different [M]-CAL-2 samples, independently of the type and concentration of the transition metal source used during the synthesis, presented the same crystals rhombohedra morphology observed by scanning electron microscopy (Figure 4), typical for chabasite-like materials.

For the samples using Co or Mn it can be observed that the crystal size diminishes with the increasing of the metal concentration in the precursor gel, as shown in Figure 4. Nucleation effects during the hydrothermal treatment step are probably affecting the crystal size. When the reactants are in high concentration more nucleation sites can be formed that in turn grow less individually. In the case of the synthesized materials the transition metal amount added during the preparation of the synthesis gel is the unique parameter whose concentration changed during the studies, and it is probably responsible for the different nucleation rate and the respective size changing effects on the crystals.

There is also a relation between the crystal sizes and the relative crystallinity calculated from the XRD patterns. When the crystals are larger the amount of structural heteroatoms (transition metal atoms) is lower resulting in samples with fewer distortions. More crystalline samples have probably a better organized structure favoring larger crystals.

For the samples containing iron at M/Al_2O_3 molar ratio equal 0.22 and 0.33 this relationship is not observed. In these cases, other factors may be responsible for the observed differences; the preferential formation of a different iron rich phase is one possible reason (see later).

A careful view of the crystals in Figure 5 showed that they have a lamellar appearance in some of their sides indicating that the precursor to final product formation occurs mainly due to a localized transformation and rearrangement of the lamellar aluminophosphate [8,28,29]. This feature may be extremely important for the use of these materials as catalysts since this lamellar memory effect may improve the diffusional processes and the active sites availability during the catalytic reactions.

The composition of the inorganic structure of the [M]-CAL-2 (Table 3) was calculated from energy dispersive spectroscopy measurements and considering the chabazite unit cell as having the $T_{36}O_{32}$ composition.

It can be observed that for the [Co]-CAL-2 and [Mn]-CAL-2 samples there is an increase in the amount of the transition metal atoms per unit cell when higher concentration of them are used during the synthesis. This result supports the considerations about the relative crystallinity, where larger distortions were possibly related to higher concentrations of transition metals in the structure of the [M]-CAL-2. For those two groups of materials there is a linear relation between the concentrations of the transition metal (M/Al_2O_3) in the synthesis gel and its final amount in the molecular

sieve structure as revealed in Figure 6. This relationship is important since the transition metal atoms in the structure of these materials are responsible for redox and/or acid sites with special applications in the catalysis field. The control of the transition metal concentration using experimental parameters, as performed in the present work, plays an important role in the tuning of the properties of these structures to be employed in catalytic reactions.

It will be shown by the DR-UV-Vis spectroscopy (see later) that the transition metals are essentially in framework sites, in tetrahedral geometry; no signal of octahedral transition metal sites were observed, suggesting that no extraframework heteroatom is observed in these solids. [Fe]-CAL-2 materials presented a different behavior regarding crystal sizes and structural distortions related to transition metal concentration. Observing the scanning electron microscopy images from the [Fe]-CAL-2 sample with the highest iron concentration (0.33, M/Al_2O_3), presented in Figure 7, it is possible to verify the existence of the chabazite rhombohedra-like crystals and other particles without defined morphology (indicated with arrows). The dispersive energy spectroscopy analysis from those unexpected particles showed that they are composed by an iron richer silicoaluminophosphate phase than the rhombohedral crystals, indicating that at high iron concentrations an iron rich co-phase is formed whose presence directly affects the iron concentrations in the synthesized chabazite-like material. This different phase is probably amorphous or has low crystallinity because no unexpected X-ray diffraction peaks were observed (Figure 1).

The global compositions of the materials were calculated using the results presented in Table 3 and the thermogravimetric results (Supporting Information). The final unit cell compositions for the samples are presented in Table 4. The synthesized materials have essentially the same number of organic template molecules inside chabazite cavity (~1.9-2.0 molecules/cavity, each chabazite unit cell has 3 cavities) as predicted by the literature [10].

The concentration of template molecules in the unit cells are inversely related to the concentration of transition metal and silicon atoms. This behavior is justified first because the main substitution pathway, related to the transition atoms, which occur on the transformation of the lamellar aluminophosphate (AlPO-kan) into the chabazite structure is of the type $Al^{3+} \rightarrow M^{2+/3+}$. When the Al^{3+} is substituted by a transition metal with oxidation number 2+ a residual negative charge is generated and therefore a positive counter charge is necessary, in this case the alkylammonium (RNH_3^+) molecule

used as template. When the transition metal in the structure has a 3+ oxidation number no negative charge is generated, and so no template molecule is necessary for charge balancing. A similar structural negative charge is generated when P^{5+} is substituted by Si^{4+} and, as discussed above, the alkylammonium cations are necessary for maintaining the structural charge neutrality. A substitution mechanism exists whereby no charge is generated: when two Si^{4+} substitute a Al^{3+}/P^{5+} pair of ions, in this case no positive counter charge is necessary, this may occur especially from Si rich samples like [Co]-CAL-2 (0.11) and [Mn]-CAL-2 (0.11) .

Taking into consideration the mentioned above and the values presented in Table 4, it is observed that the number of alkylammonium template molecules in the [Mn]-CAL-2 materials is higher than in the Co based materials. This is justified for the samples with low transition metal loading because the sum of transition metal atoms and silicon atoms present in their structures, result of more $Al^{3+} \rightarrow Mn^{2+}$ and $P^{5+} \rightarrow Si^{4+}$ substitutions during the transformation of the lamellar aluminophosphate in the MeAPSO material, and so, more negative structural charges are generated thus demanding a larger concentration of alkylamonnium cations. For the samples with higher transition metal concentration (0.22 and 0.33) other effects like silicon island formation may affect the structural charge generation.

The most widely used description of the generation and localization of negative charges in zeolite-like materials is the Lowenstein rule [30]. This rule is applied to aluminosilicate materials and predicts that two aluminum atoms cannot neighbor themselves, because in this hypothesis two negatives charges should be dislocated over the same framework oxygen,which is highly unfavorable.

Apparently the Lowenstein rule can be applied to the synthesized [M]-CAL-2 materials, with a different approach. In a general form, the increase in the concentration of M^{2+} atoms (Mn^{2+} or Co^{2+}) in the molecular sieve structure causes a decrease in the silicon amount. As explained before, both atoms in the framework of MeAPSO-like materials may generate structural negative charges.

Having in mind that there is no indication of a preferable substitution, $Al^{3+} \rightarrow M^{2+/3+}$ or $P^{5+} \rightarrow Si^{4+}$ four different substitution pathways are possible, as shown in Figure 8. In Figure 8a the substitution by an atom M^{2+} and then by a Si is represented, in this case the resulting final structure can be permitted or prohibited by Lowenstein. The substitution prohibited by Lowenstein indicates that P^{5+} atoms neighboring a M^{2+} atom cannot be substituted by Si^{4+} due the charge vicinity. This diminishes the number of

phosphorous atoms that can be substituted by silicon diminishing the final structural concentration of silicon atoms. The same conclusions can be drawn about the substitution mechanism in Figure 8b where silicon is inserted first in the framework and than followed by M^{2+}. For the [Fe]-CAL-2 materials all substitutions are Lowenstein permitted (Figure 8 c and d) because the insertion of M^{3+} atoms in Al^{3+} positions do not generate structural negative charges, so that no negative neighboring charges are possible.

Another parameter that can affect the heteroatoms substitutions ratio and respectively negative charge generation is the counterbalancing capacity of the anionic sites. In the case of the [M]-CAL-2 this is made by the alkylammonium cations. The number of organic molecules is governed mainly by the dimensions of the chabazite cavity. This behavior is confirmed verifying that the number of RNH_3^+ molecules is quite the same as the Si+M number in Table 4. The differences between the concentrations of framework heteroatoms and the concentration of organic cations are perfectly justified by the substitution mechanism where $Al^{3+} + P^{5+} \rightarrow 2\ Si^{4+}$, as discussed above, where no charge is generated in the structure and therefore no RNH_3^+ ions are necessary. Additionally the Si+P/M+Al ratio for all materials is the same indicating that the global substituted number of framework atoms in the materials is essentially constant. The expected value for this ratio is 1.0, but again the second Si substitution mechanism may change them leading to higher values.

The oxidation and coordination state of the inserted transition metal ions was studied by DR UV-Vis spectroscopy (Figure 9). The experiments were carried out both on the as-prepared materials and on the calcined ones, after an outgassing treatment necessary to remove adsorbed impurities. Moreover, repeated oxidation and reduction treatments were performed to monitor the redox properties of the metal ions.

The spectra of the as-synthesized [Co]-CAL-2 catalysts (Figure 9a) are characterized by a broad band above 32000 cm^{-1} related to charge transfer (CT) transitions from ligand to metal in tetrahedral Co^{2+} coordination. This adsorption is responsible for the dark blue color of the as-prepared samples. Accordingly, the spectra also exhibit a strong absorption in the 14000–22000 cm^{-1} region (consisting of three components with maxima at 15100, 16700, 20700 cm^{-1}) that can be assigned to the d-d transitions ($^4A_2(F) \rightarrow {}^4T_1(P)$) of framework, divalent cobalt ions in tetrahedral coordination [31]. No appreciable differences are observed among the three different

loadings. Upon calcination in O_2 the color of the samples changes to green indicating the formation of Co^{3+} sites as proposed in the literature [32-36].

The redox behavior of the [Co]-CAL-2 0.22 sample in controlled atmosphere was investigated, as reported in Figure 10a. After oxidation the sample color becomes grayish-green and a strong adsorption with maxima at 25000, 30700 appears (Figure 10a, curve a). The appearance of these bands has been explained in terms of Co^{3+} ligand-to-metal charge transfer [37,38], as also indicated by the new broad band in the near infrared region (11000-5000 cm^{-1}), assigned to the $^5E_g \rightarrow {}^5T_{2g}$ electronic transition of tetrahedrally coordinated Co^{3+} ions [32]. The coexistence of Co^{2+} in the oxidized sample can not be excluded due to the presence of the band at 45000 cm^{-1} and of the triplet in the 14000-22000 cm^{-1} range which were assigned to CT and d-d transition of the divalent cobalt ions in tetrahedral coordination, respectively.

After reduction the sample color turns back to blue, the bands at 25000 and 30700 cm^{-1} due to CT of Co^{3+} disappear, leaving only the band above 40000 cm^{-1}due to the CT of Co^{2+} and also the d-d bands in the 22000-14000 cm^{-1} range suggesting that Co^{3+} is back reduced to Co^{2+} (Figure 10a, spectra a' or b'). The reversibility of this redox behavior can be appreciated in Figure 10a. Moreover, the stability of the crystalline framework is confirmed by XRD (same Figure).

As-synthesized [Mn]-CAL-2 are white, as expected from Mn^{2+} ions in tetrahedral coordination [39]. After calcination, the samples become dark pink and after air exposition light pink. The spectra of the as-synthesized [Mn]-CAL-2 are reported in Figure 9b. They are mainly composed by a signal at high energy, between 50000 and 44000 cm^{-1}, that can be assigned to ligand-to-metal charge transfer from the HOMO in O atoms to the LUMO in Mn^{2+} ions [40]. The d-d transitions of Mn^{2+} ions (d^5 configuration) are all spin-forbidden and thus the corresponding bands (expected around 23000 cm^{-1}) are hardly detected [41-43].

The oxidized [Mn]-CAL-2 (Figure 10b, curve a) is characterized by an intense and broad band from 47000 to 25000 cm^{-1} due to the CT transitions from oxygen to Mn^{3+} ions, and by a weaker band between 22000 and 5000 cm^{-1} that can be assigned to the $^5E_g \rightarrow {}^5T_{2g}$ transitions of Mn^{3+} or to the $^4A_2 \rightarrow {}^4T_2$ transition in Mn^{4+} species. After reduction with H_2 [Mn]-CAL-2 samples become white, the d-d transitions disappear and the charge-transfer band (between 50000 and 35000 cm^{-1}) is found at high energy (Figura 10b, spectra a' or b'). The spectrum of the reduced samples closely reminds that of the as-synthesized [Mn]-CAL-2, confirming the reversibility of the edox cycle.

DR UV–Vis spectra (Figure 9c) of as-synthesized [Fe]-CAL-2 samples shows a strong absorption in the 47000-30000 cm^{-1} range with a tail up to 20000 cm^{-1} and a broad band centered at ca. 12000 cm^{-1}. The strong band at high energy can be explained as a ligand-metal CT from oxygen (e.g., O^{2-}) to Fe^{3+} ions in tetrahedral coordination, similarly to what observed in Fe-zeolites [44-46]. The edge position of the CT band for Fe species has been often employed in the literature as an indication of the clustering degree of Fe ions. This is in principle acceptable since the absorption of Fe_xO_y clusters shifts to low energy when particle size increases [45]. However, since the energy of the CT transitions also depends on the basicity of the ligands [44], a shift of the edge position could be also interpreted in terms of changes in the coordination sphere of the metal ions.

In the case of the samples prepared in this work, the adsorption in the 30000-18000 cm^{-1} range, being a tail of the CT band, is assigned to small Fe_xO_y clusters and/or to the iron rich aluminophosphate phase detected by EDS/SEM analysis (see above).

The band at ca. 12000 cm^{-1} has not often been observed in Fe-based catalysts. Bands in the same spectral region were reported by Solomon *et al.* [47] for magnetic circular dicroism spectra of Fe^{2+} homogeneous complexes with different symmetry. Similar spectra were measured in Fe-doped glasses and were assigned to Fe^{2+} species in octahedral coordination [48]. Keeping in mind the indication from the literature, the interpretation of the spectral features described above will be based on the transformation observed upon redox treatments.

As far as the CT $O \rightarrow Fe^{3+}$ bond is concerned, an apparent blue shift is observed in passing from the as-synthesized sample to the oxidized and finally to the reduced one. Since this band is still observable on the reduced sample, we have to infer that not all Fe^{3+} is reduced after this treatment (Figure 10c, spectra a' and b').

The shift of the edge position from the as-synthesized to the oxidized sample (Figure 10c, curve a) is accompanied by the growth of the component between 30000 and 18000 cm^{-1}, suggesting that calcination is accompanied by clustering of Fe ions. After reduction (Figure 10c, spectra a' or b'), the components between 30000 and 18000 cm^{-1}, assigned to clusters and oligomers strongly decrease, but they reappear if the sample is successively re-oxidized. This transformation can be explained with the removal of oxygen from small Fe_xO_y aggregates.

The band centered at ca. 12000 of the as-synthesized sample is reduced in intensity and shifted to 10500 cm^{-1} after oxidation treatment and does not recover the

initial intensity after reduction. Two possible interpretations can be proposed. One is that this band is related to Fe^{2+} ions in the SAPO framework, with two additional water ligands in the as-synthesized form. After thermal activation and redox treatments the Fe ions in the framework do not recover the internal octahedral symmetry, due to the removal of water molecules.

The second interpretation, in agreement with literature reports [48], is that the band at 12000 is due to small FeO particles formed during the synthesis. Upon oxidation these FeO clusters are oxidized to Fe_xO_y giving the broad adsorption between 30000 and 18000 cm^{-1}. This transformation is partially reversible: after reduction in H_2 the intensity of the band at 10500 cm^{-1} increases.

After the successive oxidation/reduction cycles minor structural alterations were verified by X-ray diffractometry. It can be observed that the chabazite-like structure is maintained, no other crystalline phases are formed during this process once that no different diffraction peaks are observed, and all samples keep their previous high crystallinity because no halo (20-30° 2θ) of amorphous phases is observed.

CONCLUSIONS

Transition metal (Co, Mn or Fe) substituted CAL-2 materials were synthesized using lamellar AlPO-kanemite as Al and P single source. The final materials had chabazite like structures analogous to SAPO-34 and typical rhomboedral morphology. The amount of transition metal salt added during the synthesis gel preparation directly affected the crystallinity and morphology of the obtained [M]-CAL-2: increased transition metal concentration led to less crystalline samples with smaller crystals' dimensions.

A relation between the substitution of both transition metal and silicon in the transformation of the AlPO-kan into [M]-CAL-2 is apparent, which was discussed in terms of a directed behavior similar to the Lowenstein rule for zeolites. The oxidation state of the transition metal ions may play an important role on the control of the overall substitution: when +2 state metals (Co^{2+} or Mn^{2+}) were used more structural negative charges may be generated restricting the number of available substitution sites for the silicon atoms due to charge restrictions. When Fe^{3+} (possibly true for other M^{+3} metal ions) was used no residual charge is expected and therefore more silicon substitution was possible.

Finally, the transition metal behavior in the molecular sieves structures was investigated by UV-Vis analysis that revealed that they are in framework tetrahedral coordination. Oxidation/reduction cycles were performed to prove the efficient redox behavior of the synthesized material and no important structural changes were observed due the redox processes, opening opportunities on the use of the [M]-CAL-2 as redox catalysts.

REFERENCES

[1] H.O. Pastore, Quim. Nova 19 (1996) 372.

[2] Y.J. Lee, H. Chon, Microporous Mater. 11 (1997) 253.

[3] N. Venkatathri, S.G. Hedge, V. Ramaswamy, S. Sivasanker, Microporous Mesoporous Mater.23 (1998) 277.

[4] Ø.B. Vistad, E.W Hansen, D.E. Akporiaye, K.P. Lillerud, J. Phys. Chem. A 103 (1999) 2540.

[5] Ø.B. Vistad, D.E Akporiaye, K.P. Lillerud, J. Phys. Chem. B 105 (2001) 12437.

[6] Ø.B. Vistad, D.E. Akporiaye, F. Taulelle, K.P. Lillerud, Chem. Mater. 15 (2003) 1639.

[7] S.F. Cheng, J.N. Tzeng, B.Y. Hsu, Chem. Mater. 9 (1997) 1788.

[8] H.O. Pastore, G.A.V. Martins, M. Strauss, L.G. Pedroni, G.B. Superti, E.C. de Oliveira, G. Gatti, L. Marchese, Microporous Mesoporous Mater.107(1-2) (2008) 81.

[9] A. Albuquerque, S. Coluccia, L. Marchese, H.O. Pastore, Stud. Surf. Sci. Catal. 154 (2004) 966.

[10] C. Gieck, C. Bisio, L. Marchese, Y. Filinchuk, C.E. da Silva, H.O. Pastore, Angew. Chem. Int. Edit. 46(46) (2007) 8895.

[11] H.O. Pastore, G.A.V. Martins, G.B. Superti, M. Strauss, L. Marchese, Patent Application INPI018060038592 (2006).

[12] C. Gieck, G.A.V. Martins, H.O. Pastore, L. Marchese, Stud. Surf. Sci. Catal. 174 (B) (2008) 917.

[13] G.A.V. Martins, H.O. Pastore, Microporous Mesoporous Mater.116 (1-3) (2008) 131.

[14] E.C. Oliveira and H.O. Pastore, non published results.

[15] H.O. Pastore, S. Coluccia, L. Marchese, Annu. Rev. Mater. Res. 35 (2005) 351.

[16] D.L Felix, M. Strauss, L.C. Ducati, H.O Pastore, Microporous Mesoporous Mater.120(3) (2009) 187.

[17] B. Palella, M. Cadoni, A. Frache, H.O. Pastore, R. Pirone, G. Russo, S. Coluccia, L. Marchese, J. Catal. 217 (2003) 100.

[18] S.T. Wilson, E.U. Flanigen, U.S. Patent Application 4,567,029, (1986).

[19] E.U. Flanigen, B.M. Lok, S.T. Wilson,, , R.L. Patton, Pure Appl. Chem. 58 (1986) 1351.

[20] Database of Zeolite Structures in http://www.iza-online.org.

[21] D. Ciuparu, M.R. Lyubovsky, E. Altman, L.D. Pfefferle, A. Datye, Catal. Rev. 44 (2002) 593.

[22] K. Eguchi, H. Arai, Catal. Today 29 (1996) 379.

[23] P. Gélin, M. Primet, Appl. Catal. B-Environ. 39 (2002) 1.

[24] P. Forzatti, G Groppi, Catal. Today 54 (1999) 165.

[25] National Institute of Standarts and Technology, in http://webbook.nist.gov/cgi/cbook.cgi?Name=methane&Units=SI, January/2008.

[26] O.V. Yakubovich, W. Massa, P.G. Gavrilenko, I.V. Pekov, Crystallogr. Rep. 50 (2005) 544.

[27] M. D'Amore, C. Bisio, G. Talarico, M. Cossi, L. Marchese, Chem. Mater. 20 (2008) 4980.

[28] H.O. Pastore, E.C. de Oliveira, G.B. Superti, G. Gatti, L. Marchese, J. Phys. Chem. C, 111 (2007) 3116.

[29] M. Milanesio, G. Croce, A. Frache, L. Marchese, D. Viterbo, C.E. da Silva, E.C. de Oliveira, H.O. Pastore, Stud. Surf. Sci. Catal., 158 (2005) 311.

[30] W. Loewenstein, Am. Mineralogist, 39 (1954) 92.

[31] M. Hartmann, L. Kevan, Chem. Rev. 99(3) (1999) 635.

[32] L. Marchese, G. Martra, N. Damilano, S. Coluccia, J. M. Thomas, Stud. Surf. Sci. Catal. 101 (1996) 861.

[33] R.A. Schoonheydt, R. De Vos, J. Pelgrims, H. Leeman, Stud. Surf. Sci. Catal. 49 (1989) 559.

[34] K. Y. Lee, M. Chon, J. Catal. 126 (1990) 667.

[35] B. Kraushaar-Czarnetszki, W. G. Hoogervorst, R. R. Andrea, C. A. Emeis, W. H. J. Stork, J. Chem. Soc. Faraday Trans. 87 (1991) 891.

[36] K. Nakashiro, Y. Ono, Bull. Chem. Soc. Jpn. 66 (1993) 9.

[37] L. Canesson, A. Tuel, Zeolites 18 (1997) 260.

[38] N. Rajié, I. Arcon, V. Kaucic, A. Kodre, Croatica Chem. Acta 72 (1999) 645.

[39] Y. Wei, Y. He, D. Zhang, L. Xu, S. Meng, Z. Liu, S. Bao-Lian, Micropor. Mesopor. Mat. 90 (2006) 188.

[40] B. Modén, L. Oliveiro, J. Dakka, J.G. Santiesteban, E. Iglesia, J. Phys. Chem B 108 (2004) 5552.

[41] S.B. Hong, S.J. Kim, Y.S. Choi, Y.S. Uh, Stud. Surf. Sci. Catal. 105 (1997) 779.

[42] W.S. Kijlstra, E.K. Poels, A. Bliek, B.M. Weckhuysen, R.A. Schoonheydt, J. Phys. Chem B 101 (1997) 309.

[43] N. Rajic, D. Stojakovic, S. Hocevar, V. Kaucic, Zeolites 13 (1993) 384.

[44] B.N. Figgis, Introduction to Ligand Fields, Wiley, New York, 1966.

[45] S. Bordiga, R. Buzzoni, F. Geobaldo, C. Lamberti , E. Giamello, A. Zecchina, G. Leofanti, G. Petrini, G. Tozzola, G. Vlaic, J. Catal. 158 (1996) 486.

[46] M.S. Kumar, M. Schwidder, W. Grunert, A. Bruckner, J. Catal. 227 (2004) 384.

[47] E.I. Solomon, T.C. Brunold, M. I. Davis, J.N. Kemsley, S.K. Lee, N. Lehnert, F. Neese, A. J. Skulan, Y.S. Yang, J. Zhou, Chem. Rev. 100 (2000) 235.

[48] R. Carl, S. Gerlach, C. Russel, Journal of Non-Crystalline Solids 353 (2007) 244.

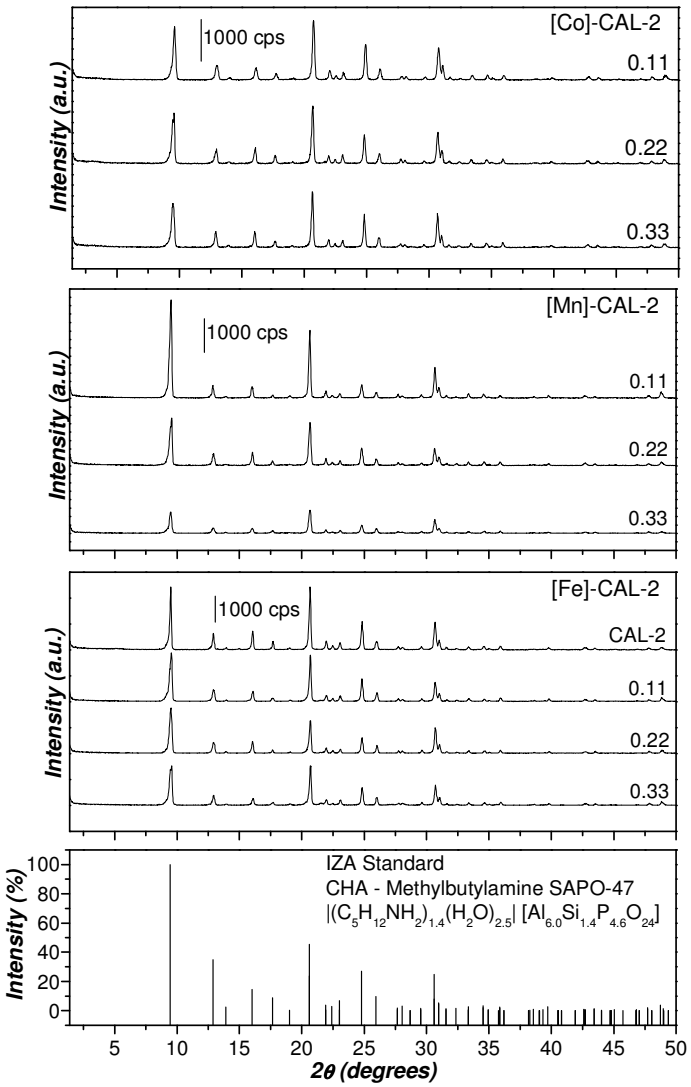

Figure 1. XRD patterns of the [M]-CAL-2 materials.

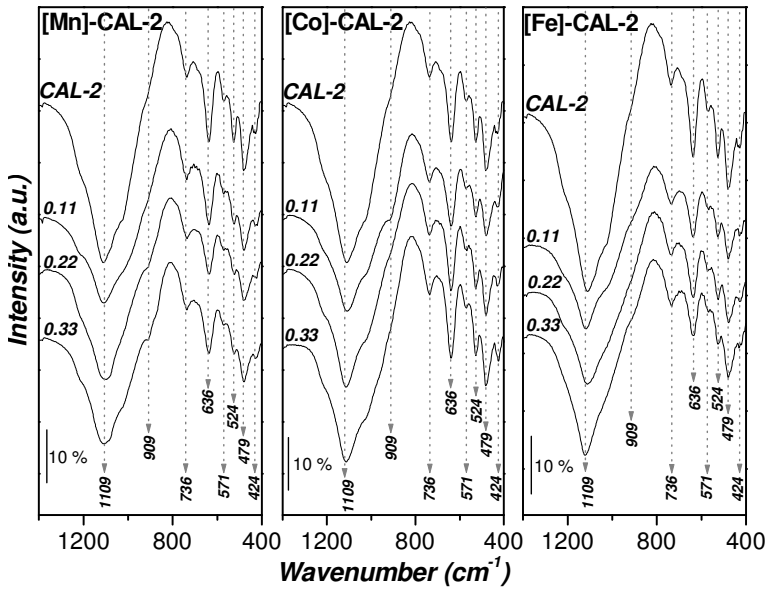

Figure 2. Infrared spectra in the region of 1400-400 cm^{-1} of the [M]-CAL-2 samples.

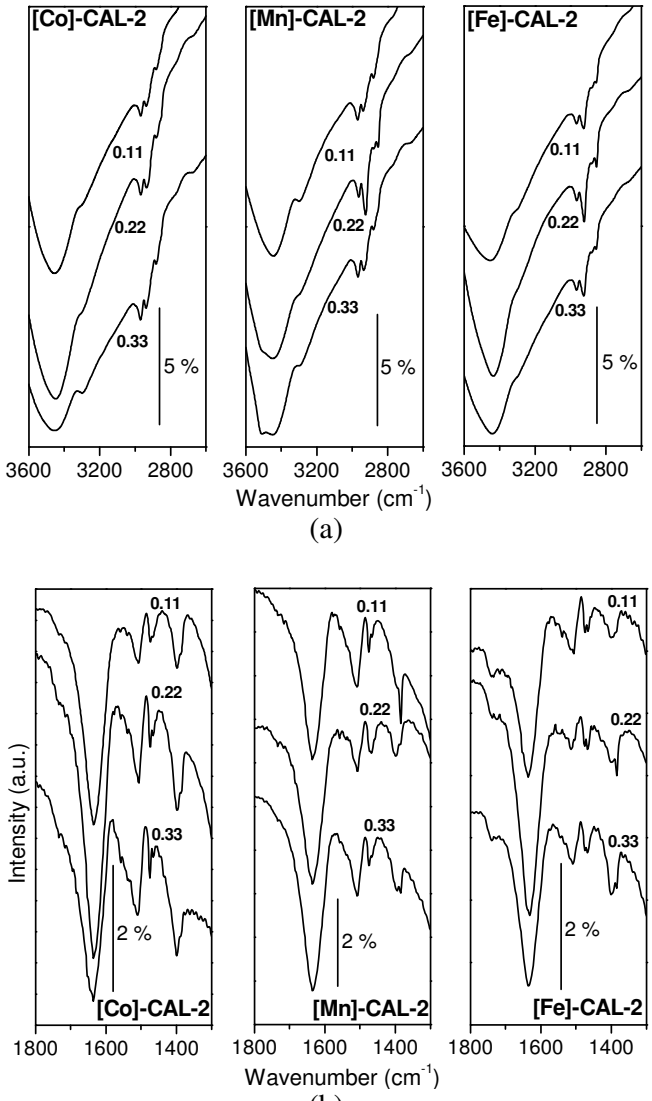

Figure 3. Infrared spectra in the region of a) 3600-2600 cm^{-1} and b) 1800-1500 cm^{-1} of the [M]-CAL-2 samples.

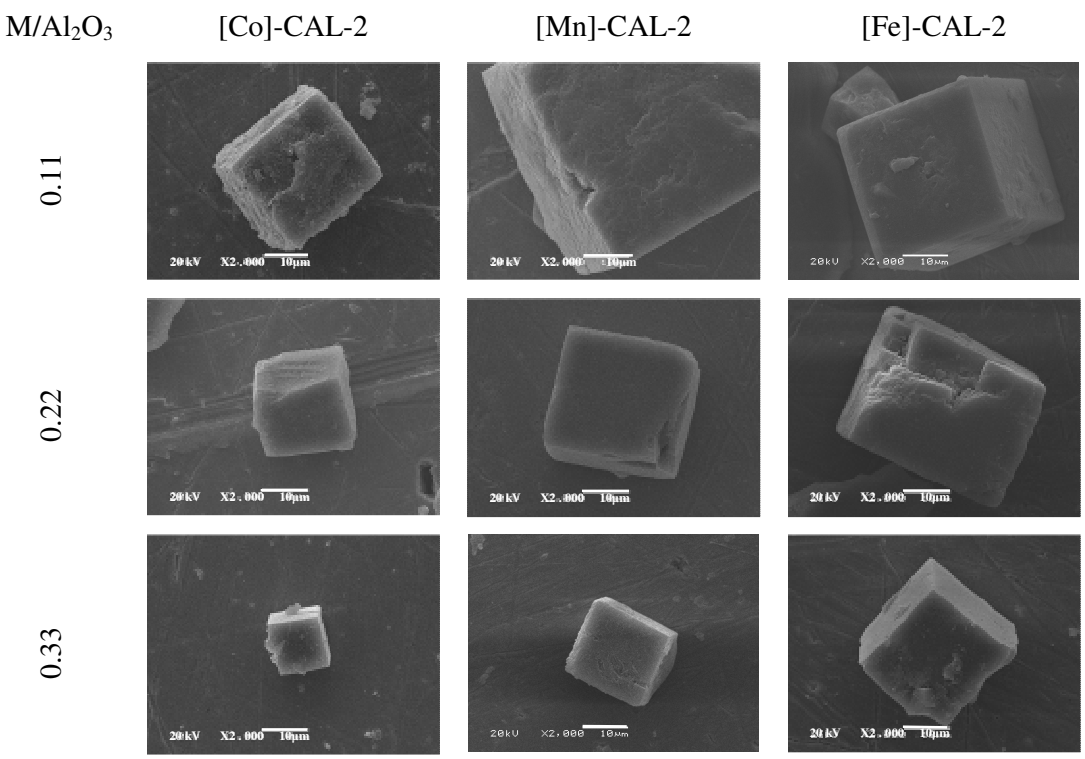

Figure 4. Scanning electron microscopy images of the various [M]-CAL-2 materials synthesized with different M/Al_2O_3 ratio.

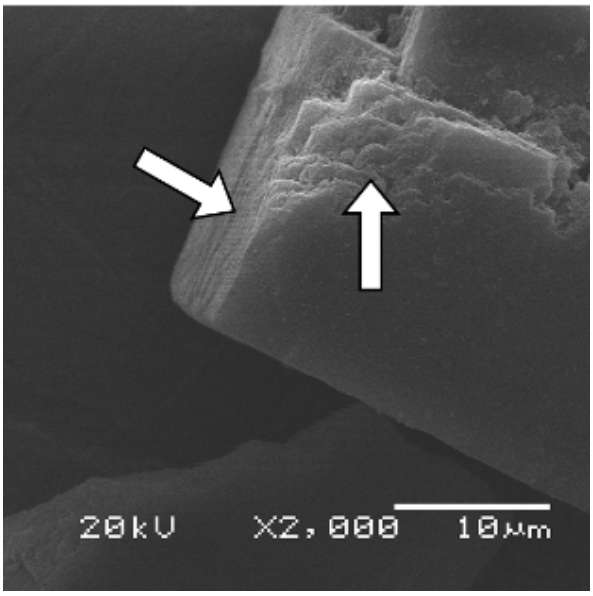

Figure 5. Evidences of lamellar appearance on the [Fe]-CAL-2 (M/Al_2O_3 = 0.22) crystals.

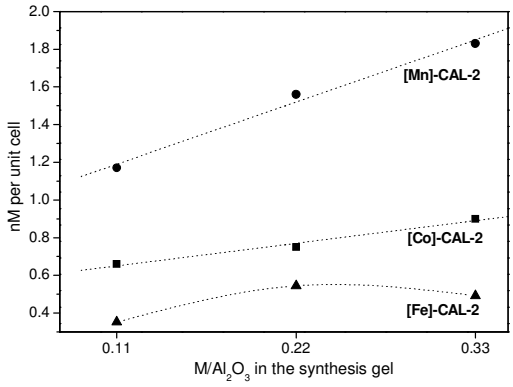

Figure 6. Calculated number of transition metal atoms per chabazite unit cell in function of the used M/Al_2O_3 ratio in the synthesis gel.

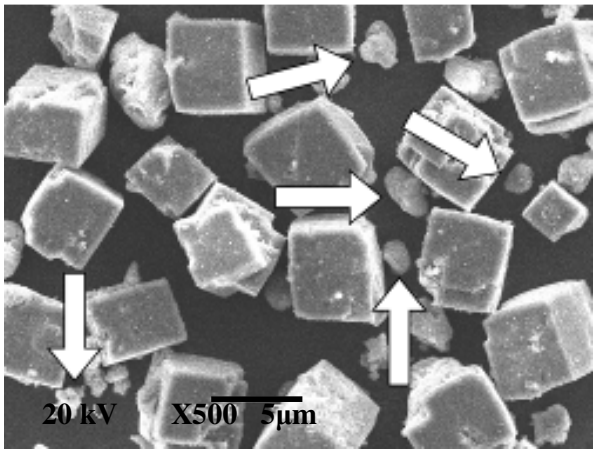

Figure 7. Scanning electron microscopy image of the [Fe]-CAL-2 sample with $M/Al_2O_3 = 0.33$.

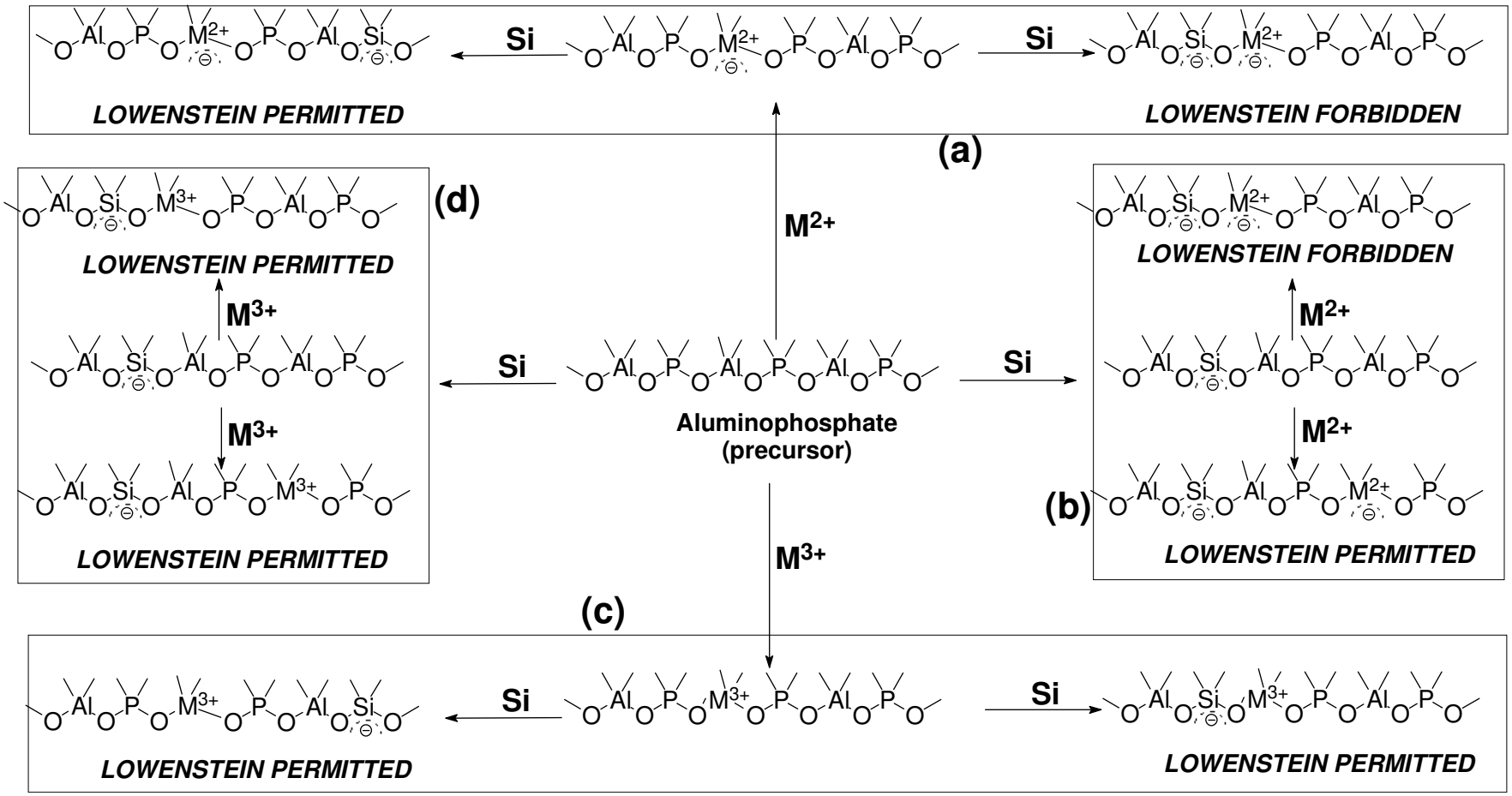

Figure 8. Lowenstein ruled possible substitution pathways ($Al^{3+} \rightarrow M^{2+/3+}$ or $P^{5+} \rightarrow Si^{4+}$) in the [M]-CAL-2 materials.

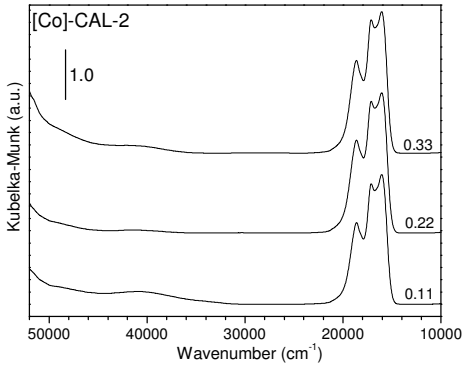

(a)

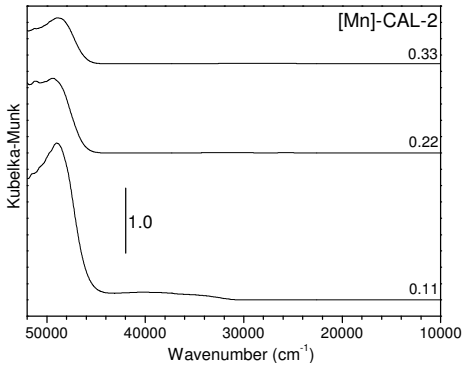

(b)

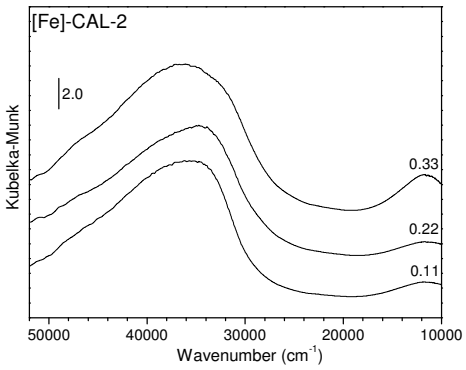

(c)

Figure 9. UV-vis spectra of the different as-synthesized [M]-CAL-2 materials where M is a) Co, b) Mn or c) Fe.

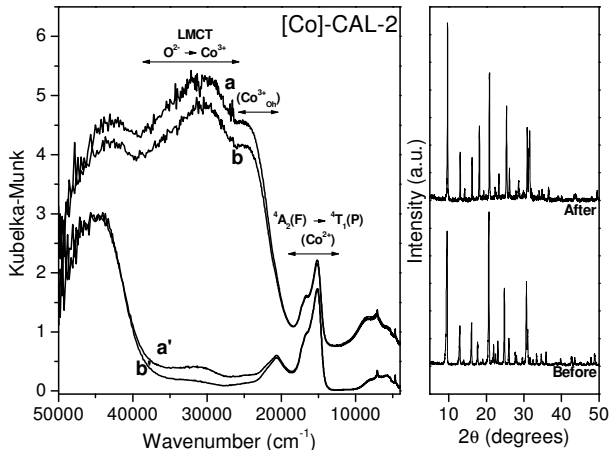

(a)

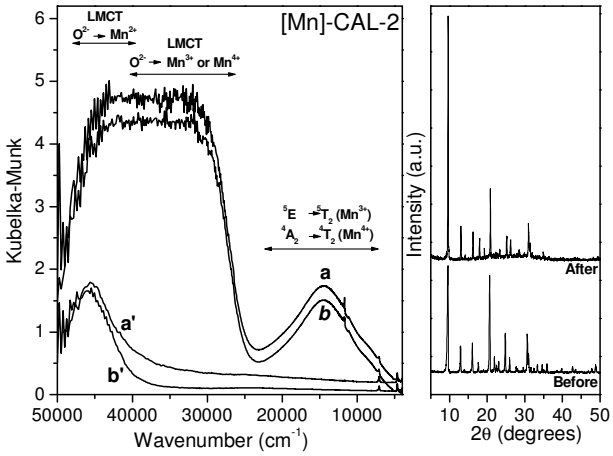

(b)

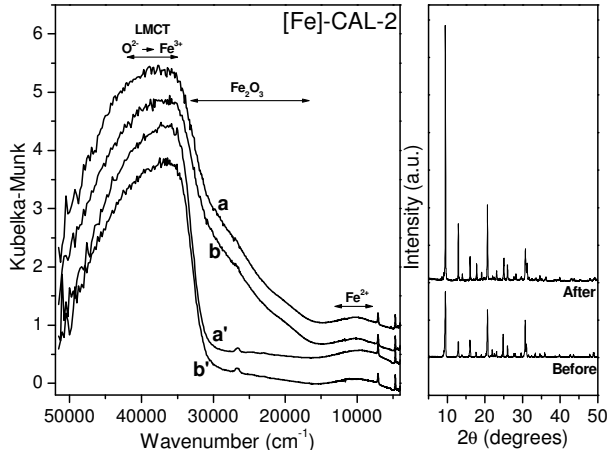

(c)

Figure 10. Successive reductive (under H_2) and oxidative (under O_2) experiments over the [M]-CAL-2 materials with M/Al_2O_3 = 0.22. All spectra labeled as a and b were obtained on oxidized samples, a' and b' on reduced ones. On the right side are shown the XRD patterns of each sample after and before the redox tests.

SUPPORTING INFORMATION

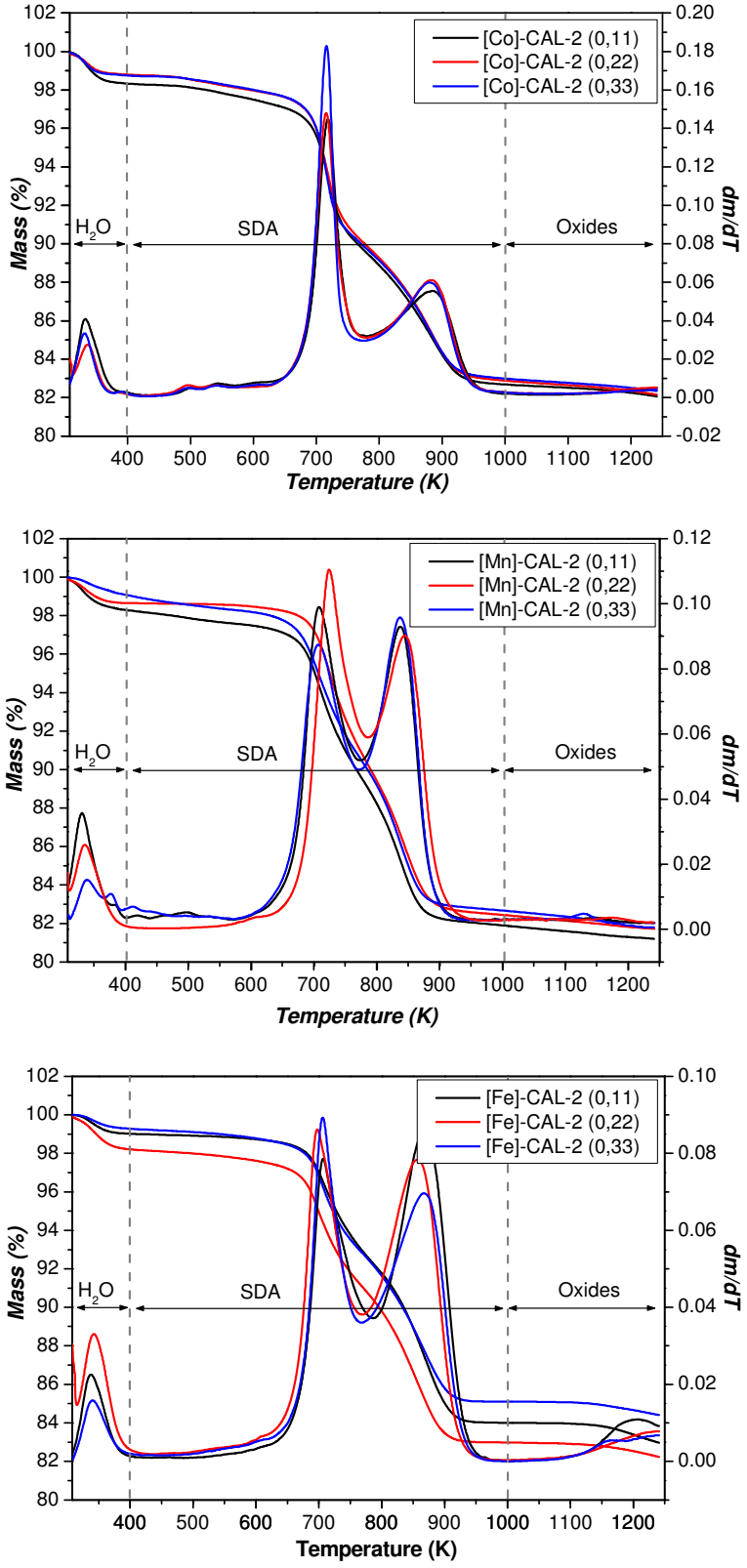

Figure 11. Thermogravimetric analysis of [M]-CAL-2 samples (M = Co, Mn or Fe).

Table 1. Integrated values of the four more intense peaks of the XRD patterns and calculated relative crystallinity (%) for the [M]-CAL-2.

Material		Integration values				Results	
[M]-CAL-2	M/Al_2O_3	20.7°	24.8°	30.6°	30.7°	Σ	%C
[Co]-	0.11	370.34	202.00	206.20	70.34	848.88	100
	0.22	324.44	156.28	191.86	70.84	743.42	88
	0.33	298.40	164.86	183.86	56.08	703.20	83
[Mn]-	0.11	375.90	89.62	198.84	66.56	730.92	100
	0.22	309.24	125.22	134.08	59.66	628.20	86
	0.33	169.46	62.74	96.86	34.94	364.00	50
[Fe]-	0.11	378.70	178.98	164.88	63.22	785.78	100
	0.22	296.16	128.74	225.60	64.88	715.38	91
	0.33	335.30	146.26	165.00	63.92	710.48	90

Table 2. Band assignments of bands present in the spectra in Figure 2 [26].

Wavenumber (cm^{-1})	Attribution
1109	ν_{as}T-O (TO_4)
909	ν_sSi-OH
736	ν_sT-O (TO_4)
636	Double 6-membered rings
571	δO-P-O (PO_4)
524	δO-T-O ($(Al,Si)O_4$)
479	δO-Si-O (SiO_4)
424	8-membered rings

Table 3. Calculated values of the inorganic composition normalized to the expected value of a chabazite unit cell of the [M]-CAL-2 materials.

	[Co]-CAL-2			[Mn]-CAL-2			[Fe]-CAL-2		
M/Al_2O_3	0.11	0.22	0.33	0.11	0.22	0.33	0.11	0.22	0.33
Al	15.77 ±0.38	15.93 ±0.40	15.62 ±0.22	15.08 ±0.36	15.18 ±0.25	14.91 ±0.38	15.89 ±0.28	15.96 ±0.27	15.77 ±0.48
Si	7.36 ±0.84	6.64 ±0.70	6.80 ±0.34	7.51 ±0.71	5.81 ±0.45	5.77 ±0.34	7.78 ±0.68	7.05 ±0.60	7.73 ±1.24
P	12.21 ±0.53	12.68 ±0.44	12.68 ±0.23	12.24 ±0.44	13.44 ±0.27	13.49 ±0.27	11.93 ±0.38	12.36 ±0.39	11.93 ±0.71
M	0.66 ±0.16	0.75 ±0.22	0.90 ±0.21	1.17 ±0.34	1.56 ±0.21	1.83 ±0.31	0.41 ±0.08	0.63 ±0.08	0.57 ±0.10
Si+P/Al+M	1.19	1.16	1.18	1.22	1.15	1.15	1.21	1.17	1.20

Table 4. Calculated global unit cell composition of the [M]-CAL-2 materials.

[M]-CAL-2 (x)[a]	M+Si	Unit cell
[Co]-CAL-2 (0.11)	8.02	$5.63(RNH_3^+)\ Co_{0.66}\ Si_{7.36}\ Al_{15.77}\ P_{12.21}\ O_{72}.2.47H_2O$
[Co]-CAL-2 (0.22)	7.39	$5.72(RNH_3^+)\ Co_{0.75}\ Si_{6.64}\ Al_{15.93}\ P_{12.68}\ O_{72}.1.77H_2O$
[Co]-CAL-2 (0.33)	7.70	$5.67(RNH_3^+)\ Co_{0.90}\ Si_{6.80}\ Al_{15.62}\ P_{12,68}\ O_{72}.1.86H_2O$
[Mn]-CAL-2 (0.11)	8.68	$5.94(RNH_3^+)\ Mn_{1.17}\ Si_{7.51}\ Al_{15.08}\ P_{12.24}\ O_{72}.2.05H_2O$
[Mn]-CAL-2 (0.22)	7.37	$6.07(RNH_3^+)\ Mn_{1.56}\ Si_{5.81}\ Al_{15.18}\ P_{13.44}\ O_{72}.2.68H_2O$
[Mn]-CAL-2 (0.33)	7.60	$6.02(RNH_3^+)\ Mn_{1.83}\ Si_{5.77}\ Al_{14.91}\ P_{13.49}\ O_{72}.1.53H_2O$

[a][Fe]-CAL-2 samples were not examined due to the presence of iron rich phases, see below.

SUPPORTING INFORMATION FOR

[M]-CAL-2: MeAPSO-34-like molecular sieves using a lamellar aluminophosphate as precursor

Mathias Strauss[1], Gesley Alex Veloso Martins[2], Gloria Berlier[2], Salvatore Coluccia[2], Leonardo Marchese[3], Heloise O. Pastore[1,*]

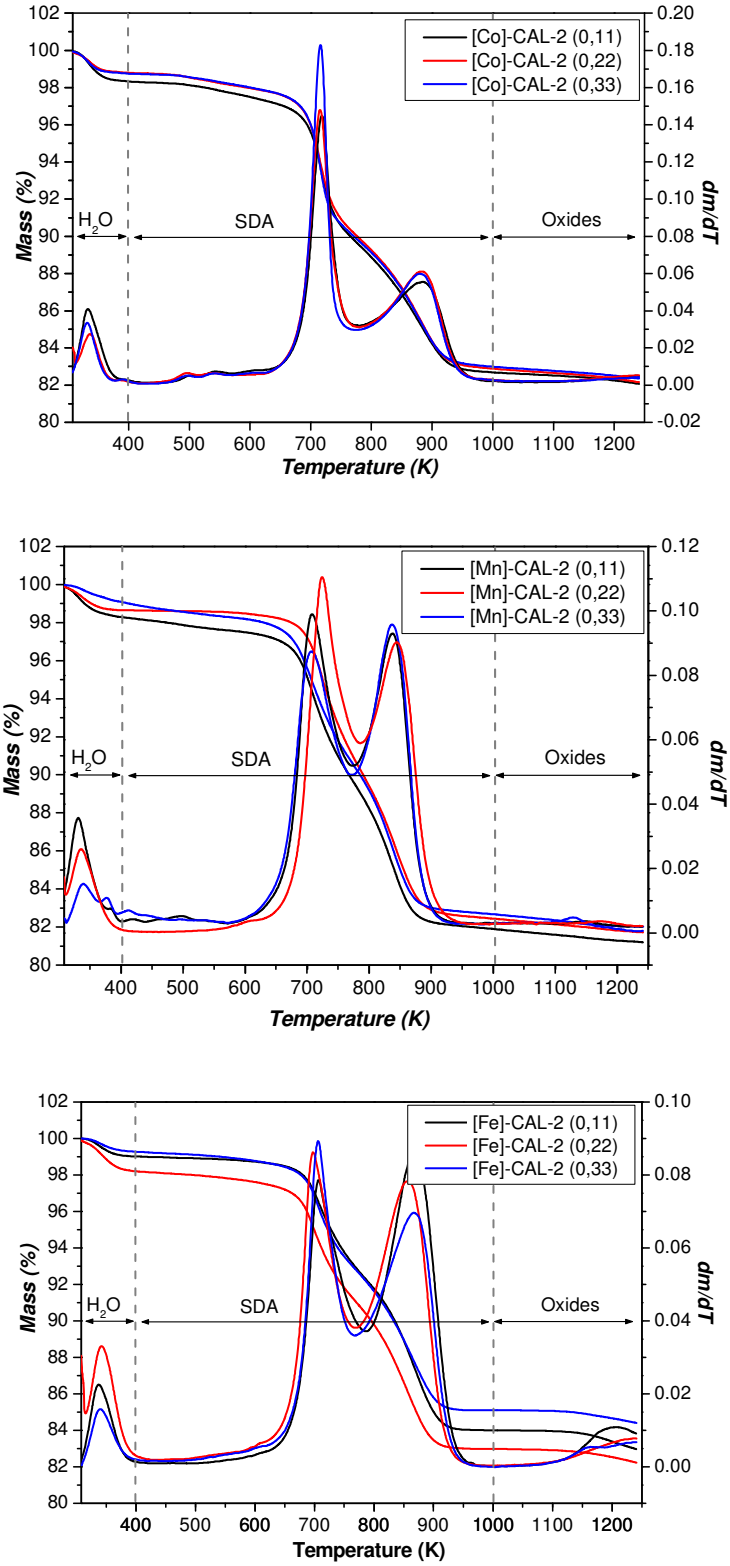

Figure S1. Thermogravimetric analysis of [M]-CAL-2 samples (M = Co, Mn or Fe).